




Article

Stability and function of RCL1 are dependent on the interaction with BMS1

Yong Wang ^{1,†,*}, Zhenyu Zhao ^{2,†}, Hongyan Yu ², Hui Shi², Boxiang Tao², Yinan He², Jun Chen³, Jinrong Peng ², Meifu Gan^{1,*}, and Li Jan Lo^{2,*}

¹ Pathology Department of Taizhou Hospital, Zhejiang University, Taizhou 317000, China

² MOE Key Laboratory for Molecular Animal Nutrition, College of Animal Sciences, Zhejiang University, Hangzhou 310058, China

³ College of Life Sciences, Zhejiang University, Hangzhou 310058, China

[†] These authors contributed equally to this work.

* Correspondence to: Yong Wang, E-mail: wangy5352@enzemed.com; Meifu Gan, E-mail: ganmf@enzemed.com; Li Jan Lo, E-mail: g0403022@zju.edu.cn

Edited by Anming Meng

During ribosome biogenesis, the small subunit (SSU) processome is responsible for 40S assembly. The BMS1/RCL1 complex is a core component of the SSU processome that plays an important role in 18S rRNA processing and maturation. Genetic studies using zebrafish mutants indicate that both Bms1-like (Bms1l) and Rcl1 are essential for digestive organ development. In spite of vital functions of this complex, the mutual dependence of these two nucleolar proteins for the stability and function remains elusive. In this study, we identified an RCL1-interacting domain in BMS1, which is conserved in zebrafish and humans. Moreover, both the protein stability and nucleolar entry of RCL1 depend on its interaction with BMS1, otherwise RCL1 degraded through the ubiquitination–proteasome pathway. Functional studies revealed that overexpression of RCL1 in BMS1-knockdown cells can partially rescue the defects in 18S rRNA processing and cell proliferation, and hepatocyte-specific overexpression of Rcl1 can resume zebrafish liver development in the *bms1l* substitution mutant *bms1^{sq163/sq163}* but not in the knockout mutant *bms1^{pju1/zju1}*, which is attributed to the nucleolar entry of Rcl1 in the former mutant. Our data demonstrate that BMS1 and RCL1 interaction is essential for not only pre-rRNA processing but also the communication between ribosome biogenesis and cell cycle regulation.

Keywords: BMS1, RCL1, ribosome biogenesis, ubiquitination, liver development, zebrafish

Introduction

In eukaryotic cells, ribosomes function as the machinery for mRNA translation and protein synthesis. Ribosome is composed of two subunits: the 60S large subunit (LSU) and the 40S small subunit (SSU) (Ben-Shem et al., 2011; Henras et al., 2015; Khatter et al., 2015). The LSU contains 28S, 5.8S, 5S rRNAs and nearly 50 ribosomal proteins, while the SSU contains 18S rRNA and nearly 30 ribosomal proteins (Ben-Shem et al., 2011; Henras et al., 2015; Khatter et al., 2015). The 18S, 28S, and 5.8S rRNAs are encoded by the polycistronic 47S pre-rRNA gene, which is transcribed as a single transcript from rDNA loci (Henras et al., 2015; Tao et al., 2020). The processing and maturation

of 18S, 28S, and 5.8S rRNAs, which include sequential removal of internal transcribed spacer (ITS) and external transcribed spacer (ETS) by endonuclease and exonuclease cleavages, are accomplished in different parts of nucleolus (Boisvert et al., 2007; Henras et al., 2015). In yeast, there are ~200 factors, including nucleolar proteins and small nucleolar RNAs, participate in the assembly of each subunit (Charette and Baserga, 2010; Woolford and Baserga, 2013; Bohnsack and Bohnsack, 2019; Singh et al., 2021). The SSU processome, which contains several sub-complexes, including UTP-A, UTP-B, Mpp10/Imp3/Imp4, Bms1/Rcl1, and U3 snoRNP modules, is responsible for the maturation of 18S rRNA and initial assembly of SSU (Henras et al., 2015; Kornprobst et al., 2016; Chaker-Margot et al., 2017; Zhao et al., 2021). Structural study revealed that the BMS1/RCL1 complex is a core component of the SSU processome (Kornprobst et al., 2016; Cheng et al., 2017; Singh et al., 2021).

Previous study in yeast found that depletion or inactivation of Rcl1 leads to growth arrest and impaired pre-rRNA processing at sites A(0), A(1), and A(2), inducing a strong decrease in 18S rRNA

Received February 25, 2023. Revised July 3, 2023. Accepted July 13, 2023.

© The Author(s) (2023). Published by Oxford University Press on behalf of *Journal of Molecular Cell Biology*, CEMCS, CAS.

This is an Open Access article distributed under the terms of the Creative Commons Attribution-NonCommercial License (<https://creativecommons.org/licenses/by-nc/4.0/>), which permits non-commercial re-use, distribution, and reproduction in any medium, provided the original work is properly cited. For commercial re-use, please contact journals.permissions@oup.com

and SSU levels (Billy et al., 1999, 2000). In addition, Rcl1 acts as an endonuclease cleaving pre-rRNAs at site A2, separating rRNAs destined for the SSU and LSU (Horn et al., 2011). Further study by knockdown of RCL1 in human HeLa cells and mouse 3T3 fibroblasts showed the accumulation of 18S rRNA intermediates, including 30S and 26S in humans and 34S and 29S in mice, suggesting roles of RCL1 in the processing of 5'ETS and ITS1 (Sloan et al., 2013; Wang et al., 2014; Wells et al., 2016). Rcl1 loading to pre-rRNAs requires the GTPase protein Bms1, an interacting protein identified by yeast two-hybrid screening using Rcl1 as the bait (Wegierski et al., 2001; Karbstein et al., 2005). The interaction between BMS1 and RCL1 is conserved in yeast, zebrafish, and humans (Karbstein et al., 2005; Delprato et al., 2014; Wang et al., 2016) and independent on the GTPase activity of BMS1 (Tanaka et al., 2011; Delprato et al., 2014). Structural study showed that Bms1/Rcl1 complex located between a double propeller of UTP-B and the head of 90S particle. Specifically, Bms1 is positioned in the core of the SSU processome with domains I, II, and III lodged between Rcl1 and helices 15 and 17 of the 5' domain of 18S rRNA, while domain IV interacts with helix 43 of the 3' domain of 18S rRNA (Kornprobst et al., 2016; Chaker-Margot et al., 2017; Cheng et al., 2017), suggesting Bms1 as a molecular motor that can make conformational changes within the SSU processome, hence facilitating subsequent cleavage at site A2. Our group found that both Bms1 and Rcl1 are essential for digestive system development and 18S rRNA processing in zebrafish (Wang et al., 2012; Zhu et al., 2021a), and Bms1 functions to balance rDNA transcription and replication at the S phase through its interaction with Rcl1 and Ttf1, respectively (Zhu et al., 2021b).

The importance of BMS1/RCL1 complex in pre-rRNA processing has been extensively studied; however, their mutual dependence, if any, for protein stability and function awaits probing. In this study, we found that the RCL1-interacting domain is highly reserved in zebrafish Bms1 and human BMS1 and the protein stability of RCL1 is dependent on BMS1 level. Interestingly, the abnormal pre-rRNA processing and cell growth in BMS1-knockdown cells can be partially rescued through overexpressing RCL1. We also generated transgenic zebrafish lines overexpressing Rcl1 specifically in the liver, which can partially resume liver development in *bms1^{jsq163/sq163}* but not *bms1^{zju1/zju1}* mutant, suggesting that the interaction with Bms1 is indispensable for Rcl1 nucleolar entry to exert its function in pre-rRNA processing.

Results

RCL1-interacting domain in BMS1 is conserved in zebrafish and humans

The interaction between RCL1 and BMS1 is conserved from yeast to humans (Karbstein et al., 2005; Delprato et al., 2014; Wang et al., 2016). To locate the precise domain interacting with Rcl1, we divided full-length zebrafish Bms1 into either four fragments evenly, i.e. ZB1 (1–305 aa), ZB2 (306–611 aa), ZB3 (612–917 aa), and ZB4 (918–1226 aa), or five fragments based on domain structure, i.e. ZB5 (1–359 aa),

ZB6 (360–730 aa), ZB7 (731–1226 aa), ZB8 (1–730 aa), and ZB9 (359–1226 aa) (Figure 1A). These HA-tagged Bms1 fragments were co-expressed with Myc-Rcl1 in 293T cells for co-immunoprecipitation (co-IP) assays, and only ZB3 (Figure 1B), ZB6, ZB8, and ZB9 were co-immunoprecipitated with Rcl1 (Figure 1C). Thus, the Rcl1-interacting domain in Bms1 resides at 611–730 aa, a common region shared by the four co-immunoprecipitated fragments.

By amino acid sequence alignment, we found that the 611–730 aa region of zebrafish Bms1 shares high identity (67%) to the 678–799 aa region of human BMS1 (Figure 1D). Human BMS1 was divided into HB1 (1–677 aa), HB2 (1–799 aa), HB3 (678–1283 aa), and HB4 (800–1283 aa) accordingly (Figure 1E). Co-IP assays showed that both HB2 and HB3, the 678–799 aa-containing fragments, could interact with RCL1, while HB1 and HB4 could not (Figure 1F). Furthermore, human BMS1 and zebrafish Bms1 exhibited similar interactions with RCL1 of both species (Supplementary Figure S1A). These results strongly support that the RCL1-interacting domain in BMS1 is conserved in zebrafish and humans.

Nuclear entry of RCL1 is dependent on its interaction with BMS1

While the function of Bms1 and Rcl1 interaction has been well studied in yeast (Karbstein et al., 2005; Delprato et al., 2014), we wondered whether more information can be learnt from higher vertebrates. We first examined the localization of HA-tagged zebrafish Rcl1 and the co-expressed Flag-tagged full-length Bms1 or fragment (ZB5, ZB6, ZB7, ZB8, or ZB9) in 293T cells. HA-Rcl1 was found originally located in the cytoplasm but entering the nucleus when co-expressed with full-length Bms1 (Supplementary Figure S1B). Nuclear entry of Rcl1 was also detected when co-expressed with ZB6, ZB8, or ZB9, which contains Rcl1-interacting domain, but not ZB5 or ZB7 (Supplementary Figure S1B). Interestingly, among these five Bms1 fragments all located in the nucleus, ZB5 presented nucleolar accumulation, suggesting an inherent nucleolar localization signal in the N-terminus of Bms1. However, another N-terminus-containing fragment, ZB8, did not show the detectable nucleolar accumulation (Supplementary Figure S1B). The reason behind this requires further experiments.

We also examined the localization of MYC-tagged human RCL1 and the co-expressed FLAG-tagged BMS1 or fragment (HB1, HB2, HB3, or HB4). Similarly, MYC-RCL1 was originally located in the cytoplasm but entered the nucleus when co-expressed with full-length BMS1, HB2, or HB3, which was located in the nucleus *de novo* and exhibited an interaction with RCL1 (Supplementary Figure S1C). These results demonstrated that the interaction with BMS1 is indispensable for RCL1 nuclear entry.

Human RCL1 protein stability is dependent on BMS1 protein level

To study the relationship between BMS1 and RCL1 in more details, we knocked down BMS1 by shRNA (sh08 or sh07) in two

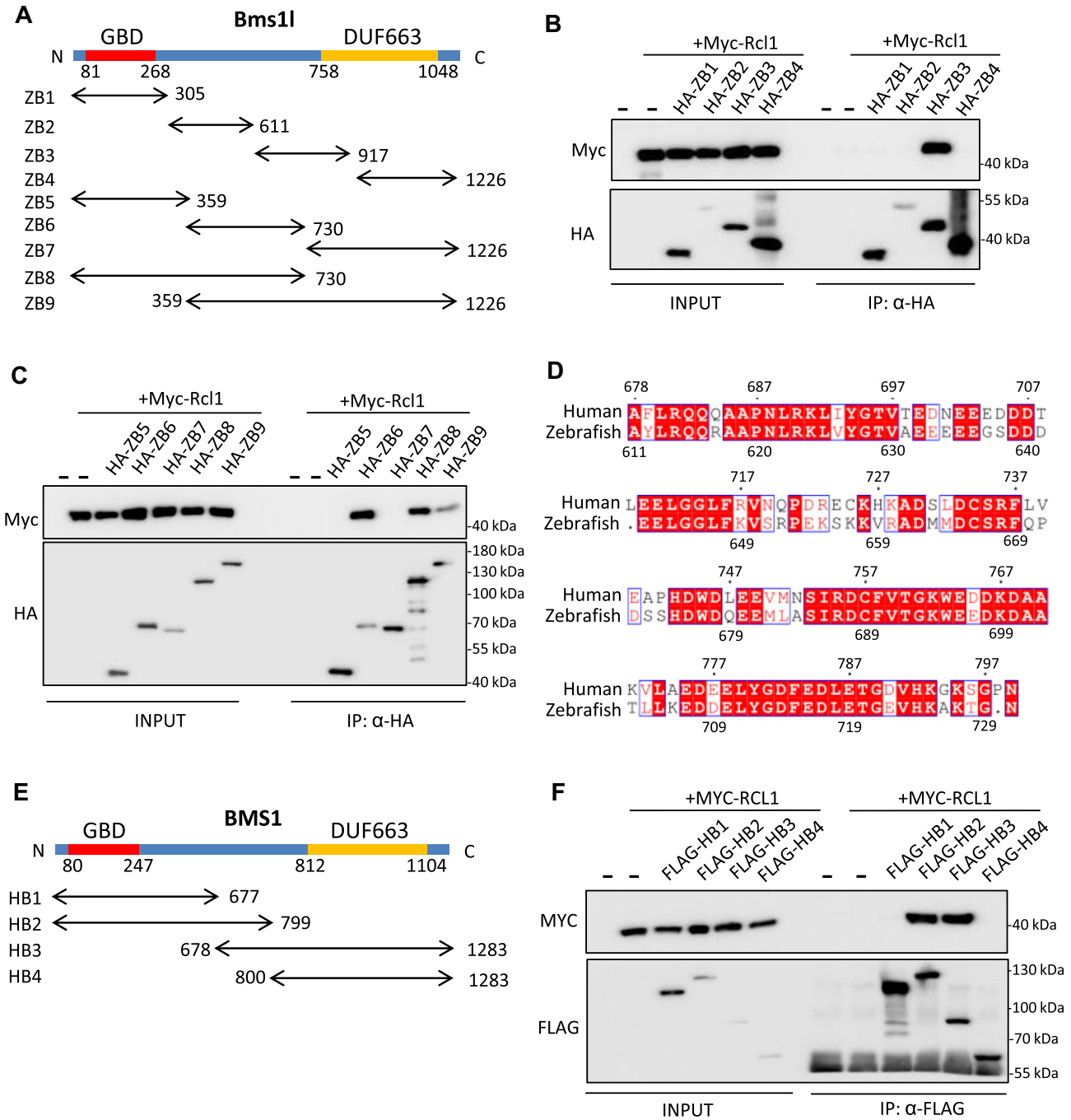


Figure 1 RCL1-interacting domain in BMS1 is conserved in zebrafish and humans. **(A)** Diagram illustrating zebrafish ZB1–ZB9. ZB1–ZB4 were divided evenly and ZB5–ZB9 were divided based on domain structure by sequence alignment with yeast Bms1. GBD, GTP-binding domain; DUF663, protein of unknown function. **(B and C)** Co-IP analysis of interactions between Myc-Rcl1 and HA-tagged ZB1–ZB4 **(B)** and ZB5–ZB9 **(C)**. HA beads were used to pull down HA-tagged ZB fragments. ZB3, ZB6, ZB8, and ZB9 interacted with Rcl1. **(D)** Amino acid sequence alignment between 611–730 aa region of zebrafish Bms11 and 678–799 aa region of human BMS1. Red boxes represent identical amino acids. **(E)** Diagram illustrating human HB1–HB4 based on predicted interacting domain. **(F)** Co-IP analysis of interactions between MYC-RCL1 and FLAG-tagged HB1–HB4. Flag beads were used to pull down FLAG-tagged HB fragments. Both HB2 and HB3 interacted with RCL1.

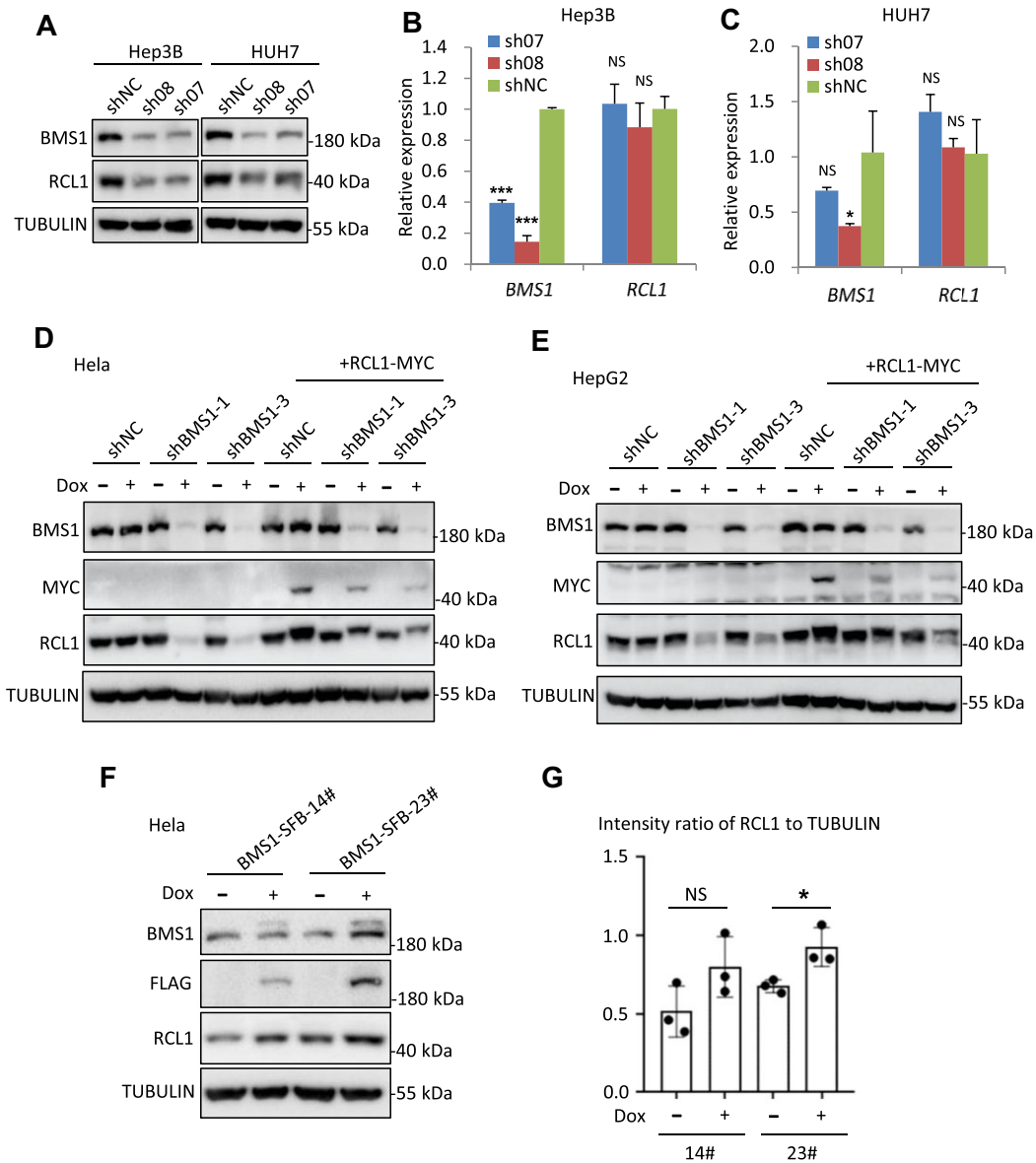


Figure 2 Human RCL1 protein stability is dependent on BMS1 protein level. **(A)** Western blot analysis of BMS1 and RCL1 protein levels in Hep3B and HUH7 cells after BMS1 knockdown by sh08 and sh07. shNC, negative control. TUBULIN: loading control. **(B and C)** qPCR analysis of the transcriptional levels of *BMS1* and *RCL1* in Hep3B **(B)** and HUH7 **(C)** cells after BMS1 knockdown by sh08 and sh07. The qPCR values were normalized against *GAPDH* and expressed as fold change of expression. **(D and E)** Western blot analysis of BMS1, RCL1 and RCL1-MYC protein levels after BMS1 knockdown and RCL1-MYC overexpression in HeLa **(D)** or HepG2 **(E)** cells by doxycycline (Dox) treatment. **(F and G)** Western blot analysis of BMS1, BMS1-SFB, and RCL1 in monoclonal HeLa cell lines (14# and 23#) with or without Dox treatment. The intensity ratio of RCL1 to TUBULIN was calculated. The data are presented as mean \pm SEM. *** $P < 0.001$; * $P < 0.05$; NS, no significance.

liver cancer cell lines, Hep3B and HUH7, and observed that while BMS1 expression was knocked down effectively, RCL1 protein level also decreased (Figure 2A). Quantitative polymerase chain reaction (qPCR) demonstrated downregulation of the transcriptional level of *BMS1* but not *RCL1* (Figure 2B and C), indicating that RCL1 was regulated at protein level. We also generated an inducible shRNA expression system to knock down BMS1 conditionally, and a Tet-On system was used to overexpress MYC-tagged RCL1 after doxycycline treatment. BMS1 was

knocked down effectively by shRNA (shBMS1-1 or shBMS1-3) in HeLa and HepG2 cells, concomitantly with a reduction in RCL1 level (Figure 2D and E). When doxycycline was added, although RCL1-MYC protein was successfully induced, its level in BMS1-knockdown cells was lower than that in normal cells (Figure 2D and E). Immunofluorescence staining demonstrated that BMS1 signal dramatically decreased in the nucleolus of HeLa (Supplementary Figure S2A) and HepG2 (Supplementary Figure S2C) cells after BMS1 knockdown. The induced

RCL1-MYC protein was located in the nucleolus of HeLa (Supplementary Figure S2B) and HepG2 (Supplementary Figure S2D) cells and not affected by BMS1 knockdown, suggesting that residual BMS1 is sufficient to complete RCL1 nucleolar transportation. However, BMS1 level was not obviously changed after RCL1 knockdown by shRNA (Supplementary Figure S2E).

Moreover, we generated two independent monoclonal HeLa cell lines (BMS1-SFB-14# and BMS1-SFB-23#) by lentivirus transfection and screening, which enable inducible expression of S-, Flag-, and SBP-tag (SFB)-tagged BMS1 (BMS1-SFB) after doxycycline treatment. We found that the protein level of RCL1 slightly increased after BMS1-SFB induction (Figure 2F and G). These data suggest that the protein level of human RCL1 is dependent on BMS1.

The protein stability of Rcl1 is dependent on Bms1l protein level in zebrafish

Next, we investigated the relationship between Bms1l and Rcl1 in zebrafish. The *bms1^{sq163/sq163}* mutant was obtained by *N*-ethyl-*N*-nitrosourea (ENU) treatment (Wang et al., 2012), harboring a T to A mutation in *bms1l* gene that leads to instability of Bms1l protein. The *bms1^{zju1/zju1}* and *rcl1^{zju1/zju1}* mutants were generated by CRISPR–Cas9, where target gene expression was shut down entirely (Zhu et al., 2021a, b). We observed that both Rcl1 and Bms1l protein levels decreased in *bms1l* mutant, while Bms1l protein level significantly increased in *rcl1* mutant (Figure 3A). We also noted that the complete loss of Rcl1 in *bms1^{zju1/zju1}* mutant was rescued in *bms1^{sq163/zju1}* double heterozygous (Supplementary Figure S3A). Immunofluorescence staining showed that Rcl1 co-localized with Bms1l in the nucleolus of wild-type (WT) hepatocytes, and Rcl1 signal intensity was greatly reduced in *bms1l* mutant (Figure 3B).

Furthermore, three independent transgenic lines with hepatocyte-specific overexpression of Myc-tagged Rcl1 were generated using Tol II transposon system (TgR1#, TgR2#, and TgR3#). qPCR and western blot analyses showed that all three lines expressed Rcl1-Myc protein in the liver, with a relatively low level in TgR3# line (Supplementary Figure S3B and C). Immunofluorescence staining showed that the Rcl1-Myc protein was specifically located in the nucleolus of hepatocytes in TgR1# and TgR3# lines (Supplementary Figure S3D). Then, TgR1# and TgR3# lines were respectively crossed with *bms1^{sq163/+}* or *bms1^{zju1/+}* mutant to probe the stability of the overexpressed Rcl1-Myc protein. The protein level of Rcl1-Myc in *bms1^{sq163/sq163}* mutant (expressing the Bms1^{sq163} mutant protein) was lower than that in siblings, while both Rcl1-Myc and endogenous Rcl1 were undetectable in *bms1^{zju1/zju1}* mutant embryos at 5 dpf (Figure 3C and D). The Rcl1-Myc protein was found to reside in the nucleolus of hepatocytes in *bms1^{sq163/sq163}* mutant (Figure 3E).

Two transgenic zebrafish lines with hepatocyte-specific overexpression of HA-tagged Bms1l (TgB1# and TgB2#) were generated using Tol II transposon system, where *bms1l*-HA expression was driven by the promoter of *fabp10a* (Supplementary

Figure S3E). Liver protein was extracted and western blot analysis showed that Rcl1 level increased in both lines (Supplementary Figure S3F). These results further demonstrated that the protein stability of Rcl1 is dependent on Bms1l protein level in zebrafish.

RCL1 can be ubiquitinated and degraded by proteasome

To explore the mechanisms behind RCL1 degradation after a reduction in BMS1 level, inhibitors leupeptin (serine and cysteine protease inhibitor), aprotinin (serine protease inhibitor), MG132 (proteasome inhibitor), pepstatin A (aspartic protease HIV protease inhibitor), bortezomib (proteasome inhibitor), tripterin (proteasome inhibitor), and 3-MA (autophagy inhibitor) were used. Hep3B and HUH7 cells after BMS1 knockdown were treated with the inhibitors for 24 h, and RCL1 protein level was recovered by MG132 and bortezomib but not the other inhibitors (Figure 4A and B), indicating that RCL1 may be degraded via the proteasome pathway (Tsubuki et al., 1996; Maclaren et al., 2001; Yerlikaya et al., 2010; Fan et al., 2011; Shahshahan et al., 2011). Similarly, *bms1^{sq163/sq163}* mutant embryos were incubated with inhibitors from 2 dpf to 5 dpf, and the Rcl1 level was rescued by MG132 and bortezomib but not pepstatin A or leupeptin (Figure 4C). These results consistently suggest that RCL1 is degraded through the ubiquitination–proteasome pathway.

Then, HA-tagged ubiquitin was co-expressed with Flag-tagged zebrafish Rcl1 or human RCL1 in 293T cells, followed by co-IP with Flag beads and immunoblotting for HA. Both Rcl1 and RCL1 were ubiquitinated by HA-tagged ubiquitin (Figure 4D). However, the ubiquitination level of human RCL1 significantly decreased when BMS1 was co-expressed (Figure 4E), hinting that BMS1 may protect RCL1 from degradation through ubiquitination masking. Five lysine residues in zebrafish Rcl1 were identified by mass spectrometry as potential ubiquitination sites. Amino acid sequence alignment demonstrated that four of them were conserved between zebrafish and humans (K126, K171, K180, and K364 in zebrafish Rcl1, corresponding to K133, K178, K187, and K370 in human RCL1) (Supplementary Figure S4). K141 in human RCL1 was also identified as a potential ubiquitination site based on mass spectrometry analysis (Elia et al., 2015). Zebrafish Rcl1 or human RCL1 with the five lysine residues mutated to arginine singly (R) or entirely (5K to R) were overexpressed in 293T cells (Supplementary Figure S5), followed by ubiquitination level detection. The mutation of K364R in zebrafish Rcl1 or K370R in human RCL1, as well as the 5K-to-R mutation in both, greatly reduced the mono- and poly-ubiquitination levels (Supplementary Figure S5). These results suggest that the conserved lysine site located at the C-terminal of RCL1 is its major ubiquitination site.

To test whether MG132 and bortezomib, two inhibitors that could rescue Rcl1 protein level, can rescue the small liver phenotype of *bms1^{sq163/sq163}* mutant, whole-mount *in situ* hybridization (WISH) was performed using liver-specific *fabp10a* probe in zebrafish at 5 dpf after inhibitor treatments. Since eye development was not significantly affected in mutant zebrafish, the

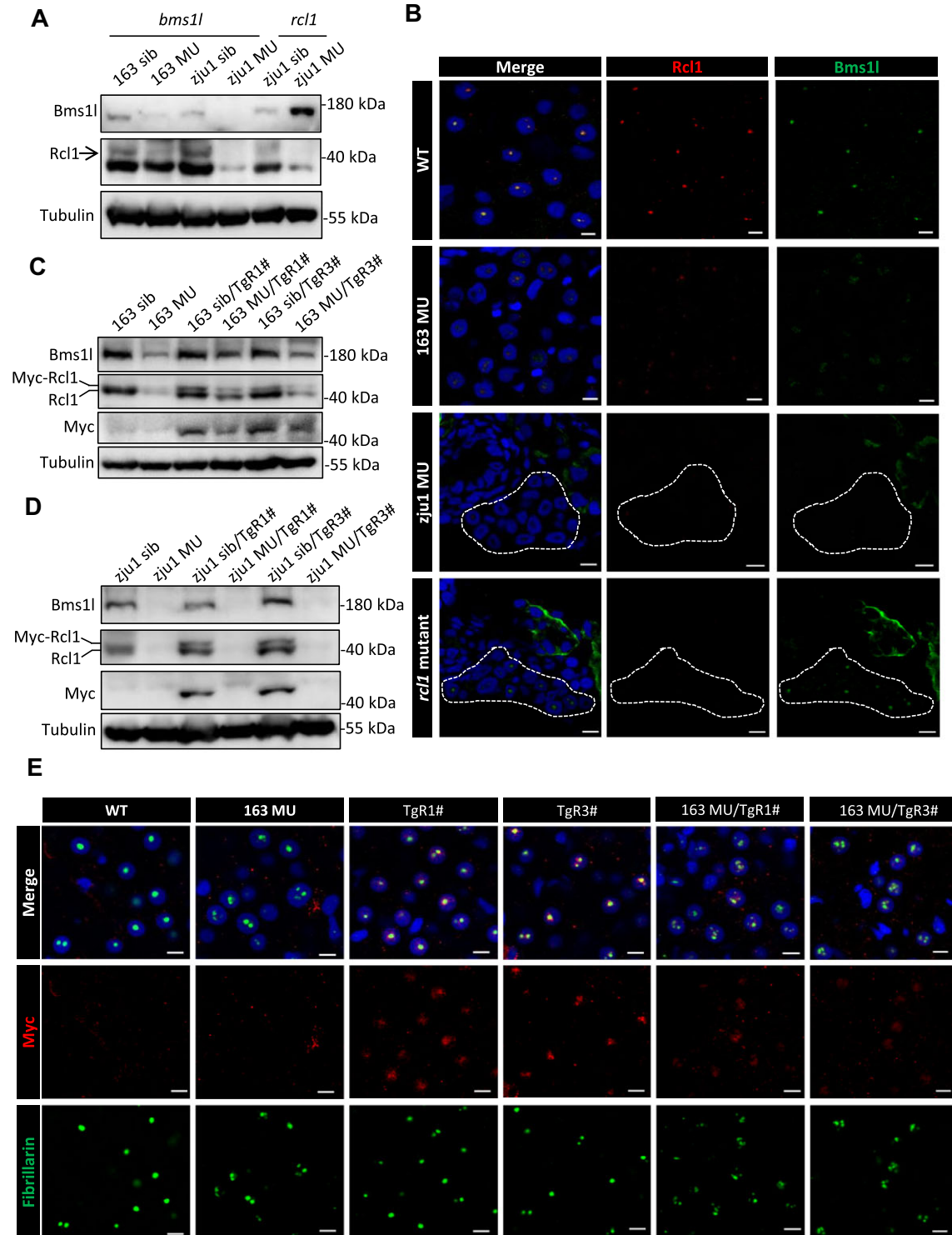


Figure 3 Protein stability of Rcl1 is dependent on Bms1l protein level in zebrafish. **(A)** Western blot analysis of Bms1l and Rcl1 protein levels in zebrafish at 5 dpf. Tubulin: loading control. 163 sib, *bms1l*^{sq163/+} and WT siblings; 163 MU, *bms1l*^{sq163/sq163} mutant; *zju1* sib, *bms1l*^{zju1/+} or *rcl1*^{zju1/+} and the corresponding WT siblings; *zju1* MU, *bms1l*^{zju1/zju1} or *rcl1*^{zju1/zju1} mutant. **(B)** Immunofluorescence staining of Rcl1 and Bms1l in WT, *bms1l*^{sq163/sq163} (163 MU), *bms1l*^{zju1/zju1} (*zju1* MU), and *rcl1*^{zju1/zju1} mutant at 5 dpf. Blue signal represents nucleus staining by DAPI. Dotted box indicates liver region. Scale bar, 5 μ m. **(C and D)** Western blot analysis of Bms1l, Rcl1 and Rcl1-Myc protein levels in *bms1l*^{sq163/sq163} mutant and siblings **(C)** or *bms1l*^{zju1/zju1} mutant and siblings **(D)** with or without the background of TgR1# or TgR3# at 5 dpf. **(E)** Immunofluorescence staining of Myc and the nucleolar marker fibrillarin to demonstrate the localization of Rcl1-Myc in hepatocytes of WT, *bms1l*^{sq163/sq163} mutant, TgR1#, TgR3#, *bms1l*^{sq163/sq163}/TgR1#, and *bms1l*^{sq163/sq163}/TgR3# at 5 dpf. Blue signal represents nucleus staining by DAPI. Scale bar, 5 μ m.

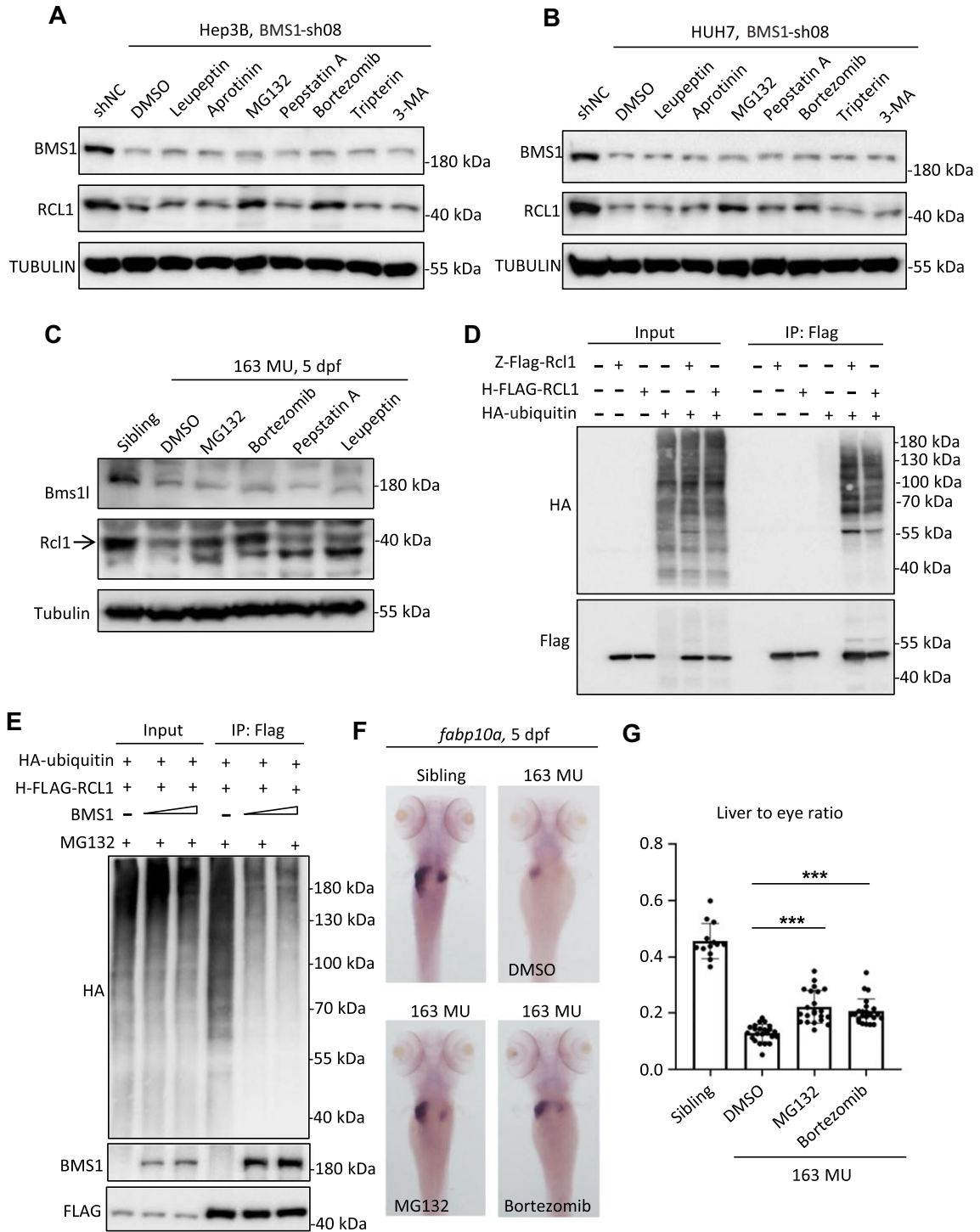


Figure 4 RCL1 is degraded through the ubiquitination–proteasome pathway. **(A and B)** After BMS1 knockdown by sh08, Hep3B **(A)** or HUH7 **(B)** cells were treated with leupeptin, aprotinin, MG132, pepstatin A, bortezomib, tripterin, or 3-MA, followed by western blot analysis to examine protein levels of BMS1 and RCL1. DMSO: negative control. **(C)** *bms1*^{sq163/sq163} mutant zebrafish were treated with MG132, bortezomib, pepstatin A, or leupeptin from 2 dpf to 5 dpf, followed by western blot analysis to examine protein levels of Bms1l and Rcl1 at 5 dpf. **(D)** Co-IP analysis of interactions between HA-ubiquitin and zebrafish Flag-Rcl1 (Z-Flag-Rcl1) or human FLAG-RCL1 (H-FLAG-RCL1). **(E)** Co-IP analysis of interactions among HA-ubiquitin, H-FLAG-RCL1, and BMS1. The transfected 293T cells were treated with MG132 for 24 h before cell harvest. **(F and G)** WISH analysis using liver-specific *fabp10a* probe in *bms1*^{sq163/sq163} mutant and siblings after MG132 or bortezomib treatment at 5 dpf. The area ratio of liver to eye was calculated. ****P* < 0.001.

area ratio of liver to eye was calculated to reflect the liver size. Both MG132 and bortezomib treatments could partially recover the small liver size in *bms1^{sq163/sq163}* mutant (Figure 4F and G), suggesting that the reduced Rcl1 level also contributes to liver dysplasia in *bms1^{sq163/sq163}* mutant.

RCL1 overexpression rescues 18S rRNA production and cell growth after BMS1 knockdown

By monitoring cell growth from 0 to 96 h, we found that growth arrest in BMS1-knockdown HeLa and HepG2 cells could be partially rescued by RCL1-MYC overexpression (Figure 5A and B).

Two pathways exist in human pre-rRNA processing, with pathway 1 playing the major role (Sloan et al., 2013; Henras et al., 2015; Figure 5C). Northern blot analysis was performed in HeLa and HepG2 cells as indicated to detect 18S rRNA production by probes P1 and P2 targeting the upstream and downstream of 18S rDNA, respectively (Figure 5C–E). After BMS1 knockdown, the intermediate products 30S/34S were accumulated, while 21S was hardly detectable, yielding a decreased production of 18S rRNA (Figure 5D and E). Overexpression of RCL1-MYC in BMS1-knockdown cells alleviated the accumulation of 30S/34S and increased the 21S level, partially rescuing the 18S rRNA production (Figure 5D and E). Consistently, the ratio of 18S to 28S rRNA, detected by Agilent 2100, significantly increased after overexpression of RCL1-MYC in BMS1-knockdown cells (Figure 5F and G). These results suggest that BMS1-dependent RCL1 protein stability is essential for 18S rRNA production and cell proliferation.

*Hepatocyte-specific overexpression of Rcl1 partially rescues liver dysplasia in *bms1^{sq163/sq163}* mutant but not *bms1^{zju1/zju1}* mutant*

To examine whether Rcl1 overexpression in the liver can rescue the small liver phenotype of *bms1l* mutant, WISH was performed using liver-specific *fabp10a* probe in offspring of *bms1^{sq163/+}/TgR1#*, *bms1^{sq163/+}/TgR3#*, *bms1^{zju1/+}/TgR1#*, or *bms1^{zju1/+}/TgR3#* at 5 dpf. The development of exocrine pancreas was also examined using the specific *trypsin* probe, and the area ratio of pancreas to eye was calculated. Our results showed significantly higher liver to eye ratios in *bms1^{sq163/sq163}/TgR1#* and *bms1^{sq163/sq163}/TgR3#* lines than in *bms1^{sq163/sq163}* mutant, while no significant difference was observed among their siblings (Figure 6A and C). In contrast, the small pancreas phenotype of *bms1^{sq163/sq163}* mutant was not rescued by hepatic expression of Rcl1 (Supplementary Figure S6A–C) and no significant difference was observed among their pancreas to eye ratios (Figure 6C). However, the *fabp10a* signal was hardly detectable in *bms1^{zju1/zju1}/TgR1#* and *bms1^{zju1/zju1}/TgR3#* lines, resembling that observed in *bms1^{zju1/zju1}* mutant (Figure 6B and D), and no significant difference was observed in either the small pancreas phenotype or the pancreas to eye ratio among these three genotypes (Supplementary Figure S6D; Figure 6D).

Next, phospho-histone H3 (PH3) immunostaining was performed to monitor the G2-to-M phase at 3 dpf. We found that PH3-positive cell ratio in the liver significantly decreased in *bms1^{sq163/sq163}* mutant compared with WT (Wang et al., 2012; Figure 6E and F), which was partially rescued by transgenic overexpression of Rcl1 in hepatocytes (Figure 6E and F). Furthermore, 5-ethynyl-2'-deoxyuridine (EdU) incorporation experiment was conducted to determine the S-phase status at 4 dpf. EdU-positive cell ratio significantly increased in the liver of *bms1^{sq163/sq163}* mutant (Zhu et al., 2021b; Supplementary Figure S6E and F), suggesting cell cycle arrest at the S phase, which was partially rescued in *bms1^{sq163/sq163}/TgR1#* and *bms1^{sq163/sq163}/TgR3#* lines. These results demonstrated that Bms1l is essential for cell cycle progression from the S to G2 phase, while overexpression of Rcl1 could partially alleviate cell cycle arrest caused by loss of function of Bms1l.

Northern blot analysis was performed to assess 18S rRNA production in adult liver total RNA by probes P3 and P4 targeting the upstream and downstream of 18S rDNA, respectively, in zebrafish pre-rRNA processing pathway 1 (Supplementary Figure S6G). Although 18S rRNA levels were similar in WT, TgR1#, and TgR3#, the levels of precursors of 18S rRNA increased in the two transgenic lines, especially pre-RNAs b and d in TgR1# (Supplementary Figure S6H), probably due to an inherently higher Rcl1-Myc expression level. Together, these results suggest that the nucleolus localization of overexpressed Rcl1-Myc is essential for rescuing liver dysplasia in *bms1l* mutant.

Discussion

The important roles of Bms1 and Rcl1 in pre-rRNA processing and SSU assembly have been described in yeast. Our work aims to extend the knowledge related to these two nucleolar proteins further into higher eukaryotes, specifically the zebrafish and human cell lines. In this study, we found that the nucleolar entry of RCL1 is dependent on its interaction with BMS1. In the absence of BMS1, RCL1 can be ubiquitinated and degraded through the proteasome pathway, leading to 18S rRNA reduction (Figure 7).

The RCL1-interacting region is conserved in zebrafish Bms1l and human BMS1 with 67% identity by amino acid sequence alignment, but shares very low identity to the 523–670 aa domain of yeast Bms1. We previously reported that zebrafish Rcl1 shares 76% identity with human RCL1 but only 37% with yeast Rcl1 (Wang et al., 2016), which may lead to the sequence differences among their RCL1-binding regions. Either zebrafish Bms1l or human BMS1 can cross interact with RCL1 of the other species, further demonstrating the conserved domain for interaction. In addition, we found that while nuclear entry of RCL1 is dependent on its interaction with BMS1, exogenously expressed RCL1, albeit interacting with endogenous BMS1, is retained in the cytoplasm. We speculate that the relatively low level of endogenous BMS1 preferentially bind with its endogenous RCL1 counterpart, resulting the cytoplasmic localization of

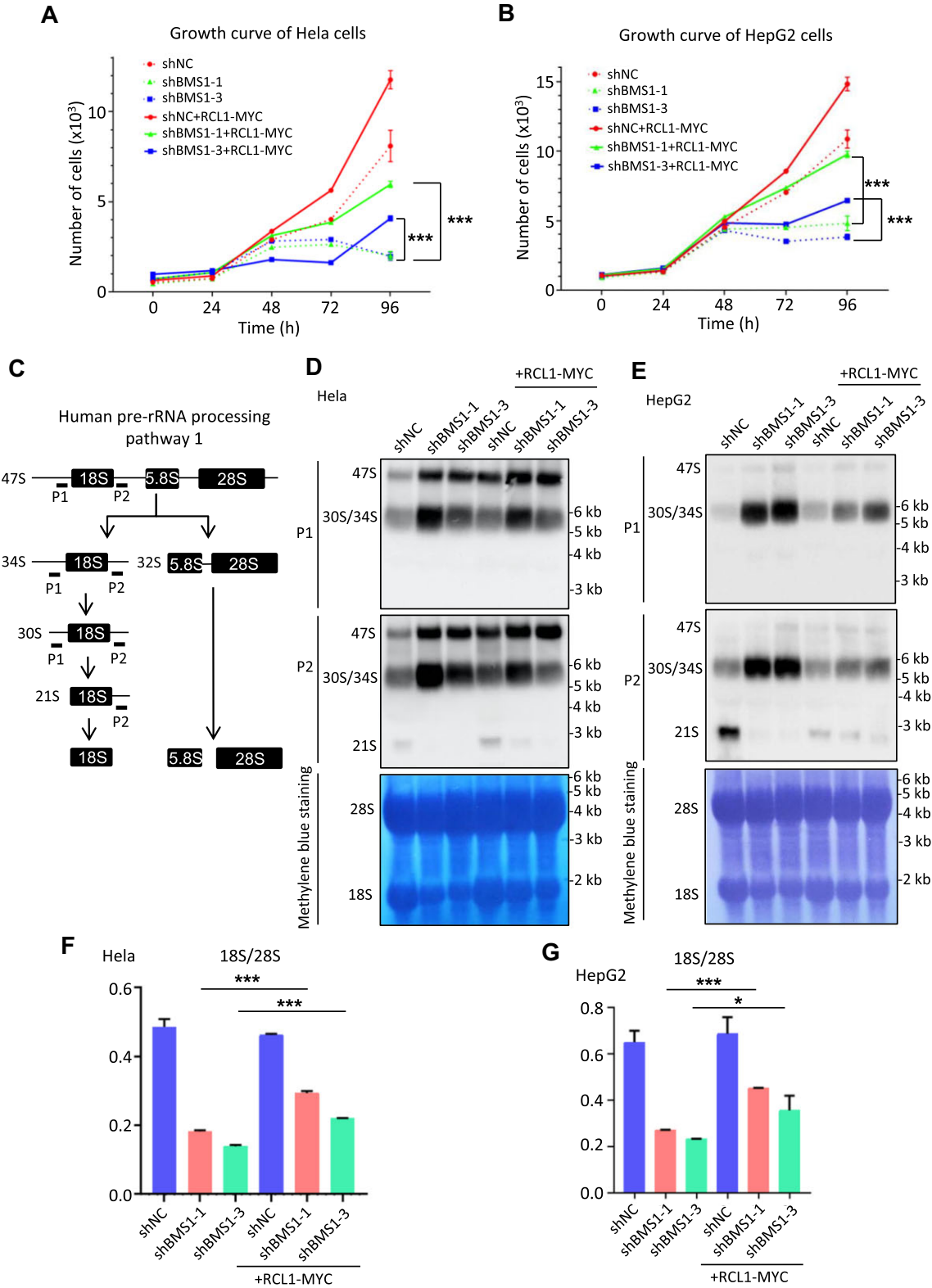


Figure 5 RCL1 overexpression rescues 18S rRNA production and cell growth after BMS1 knockdown. **(A and B)** Cell growth of HeLa **(A)** or HepG2 **(B)** cells as indicated was determined by using Cell Counting Kit-8 every 24 h from 0 to 96 h. For each time point, five repeats of one sample were set. **(C)** Diagram illustrating human pre-rRNA processing pathway 1. Probes used for northern blot analysis were shown as P1 and P2. **(D and E)** Northern blot analysis of pre-rRNA processing using biotin-labeled P1 and P2 probes in HeLa **(D)** and HepG2 **(E)** cells after doxycycline treatment. Methylene blue staining was used to indicate 28S and 18S rRNA levels. **(F and G)** Detection of 18S/28S rRNA ratio by Agilent 2100 in HeLa **(F)** and HepG2 **(G)** cells. *** $P < 0.001$; * $P < 0.05$.

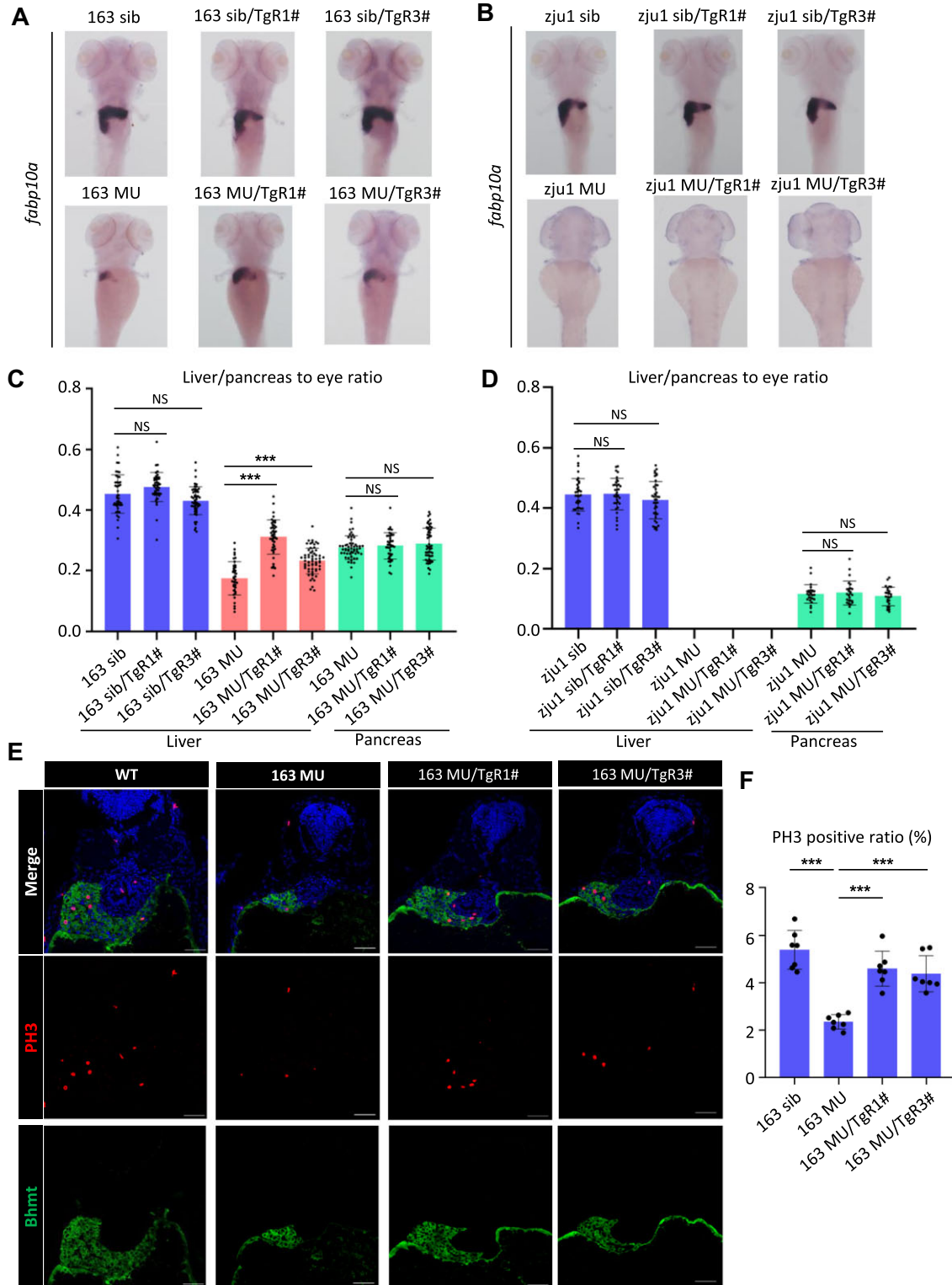


Figure 6 Hepatocyte-specific overexpression of Rcl1 partially rescues liver dysplasia in *bms1^{sq163/sq163}* mutant but not *bms1^{zju1/zju1}* mutant. (A–D) WISH was performed using liver-specific *fabp10a* probe (A and B) and the area ratio of liver or pancreas to eye was calculated (C and D) in *bms1^{sq163/sq163}* mutant and siblings (A) or *bms1^{zju1/zju1}* mutant and siblings (B) with or without the background of TgR1# or TgR3# at 5 dpf. (E and F) Immunofluorescence staining of PH3 and Bhmt (E) and the ratio of PH3-positive hepatocytes to total hepatocytes (F) in WT, *bms1^{sq163/sq163}* mutant, *bms1^{sq163/sq163}/TgR1#*, and *bms1^{sq163/sq163}/TgR3#* at 3 dpf. Bhmt is a marker of the liver and yolk. Blue signal represents nucleus staining by DAPI. Scale bar, 40 μ m. NS, no significance; *** $P < 0.001$.

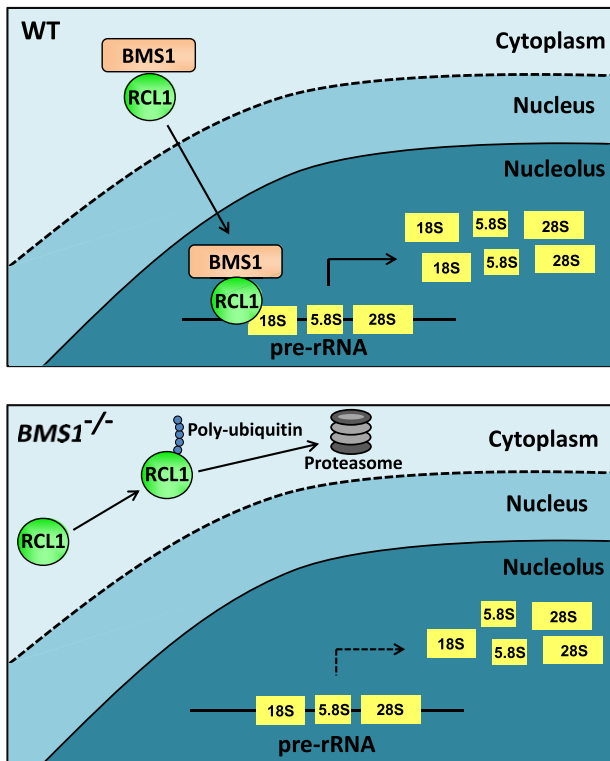


Figure 7 Schematic diagram of BMS1 and RCL1 interaction. In WT cells, RCL1 is transported into the nucleolus to execute 18S rRNA processing and maturation by interacting with BMS1 (upper). In BMS1-mutant cells, RCL1 that fails to enter the nucleus is poly-ubiquitinated and degraded by proteasome, eventually leading to the reduction of 18S rRNA level and cell growth arrest (lower).

overexpressed exogenous RCL1. Nevertheless, structural studies revealed that the BMS1/RCL1 complex is located in the core region of the SSU processome, catalyzing endonucleolytic cleavage of pre-rRNA in yeast, *Chaetomium thermophilum*, and humans (Kornprobst et al., 2016; Chaker-Margot et al., 2017; Singh et al., 2021).

We also found that RCL1 protein stability is dependent on BMS1 but not *vice versa*. Given that RCL1 is susceptible to the ubiquitination–proteasome degradation pathway, we were intrigued to characterize the potential ubiquitination sites by mutating lysine to arginine in zebrafish Rcl1 or human RCL1 and detecting their respective ubiquitination level changes, if any. The conserved C-terminal lysine site K364 in zebrafish Rcl1 (K370 in human RCL1) appears to be the major ubiquitination site. It would be interesting to find out whether this spot exists within the binding sites for BMS1 to protect RCL1 from degradation, when the two proteins interact. Recent bioinformatics analysis showed that RCL1 was downregulated during hepatocellular carcinoma (HCC) progression (Jiase et al., 2022), and we also found that Rcl1 level decreased in the liver of HCC zebrafish model (data not shown). However, the underlying mechanism is unknown. We propose that the regulation of RCL1 protein stability by ubiquitination and the interaction with BMS1 may

play a role in HCC progression, which is one of the long-term pursuits of our research team.

The GTPase domain of BMS1, acting as a molecular switch by hydrolyzing GTP, is located at the N-terminus, while RCL1-interacting domain resides in the middle region. Previous study revealed that BMS1 interacts with RCL1 independent of GTPase activity (Tanaka et al., 2011; Delprato et al., 2014). In agreement with this, both endogenous and overexpressed Rcl1 could enter into the nucleolus in *bms1^{sq163/sq163}* mutant, where the GTPase activity is impaired and the mutant protein is unstable (Zhu et al., 2021b). This was further supported by the fact that Rcl1 could not be detected in *bms1^{zju1/zju1}* mutant, where Bms1l expression is totally abolished, but the phenomenon is rescued in *bms1^{sq163/zju1}* double heterozygous.

We also explored the mechanisms underlying the characterized function of Bms1l and Rcl1 on the development of digestive organs, especially the liver, in zebrafish. Consistent with the results of functional studies in yeast, loss of function of Bms1l or Rcl1 affects pre-rRNA processing and 18S rRNA production in zebrafish (Zhu et al., 2021a, b). The p53 signaling pathway was activated in *bms1l* and *rcl1* mutant zebrafish, leading to cell cycle arrest of hepatocytes, as the positive ratio of the G2-to-M phase marker PH3 significantly decreased in the liver (Zhu et al., 2021a, b). We further demonstrated the S-phase arrest of hepatocytes in *bms1^{sq163/sq163}* mutant, leading to the high ratio of polyploidy and aneuploidy (Zhu et al., 2021b). Interestingly, transgenic overexpression of Rcl1 in the liver could alleviate S-phase arrest, partially rescuing the small liver phenotype of *bms1^{sq163/sq163}* mutant. Moreover, RCL1 overexpression rescued 18S rRNA production and cell growth after BMS1 knock-down in HeLa and HepG2 cells, suggesting a dosage requirement for RCL1 in 18S rRNA maturation, which is closely related to cell proliferation. Recently, we reported transcription termination factor 1 (TTF1) as a new interacting protein of BMS1 (Zhu et al., 2021b). We demonstrated that through its GTPase activity, BMS1 displaces TTF1 from rDNA replication fork barrier to locate down stream of 3' ETS of rDNA transcriptional unit and thus plays a role in balancing rDNA replication and transcription during the S phase, putting forward a model that the BMS1/TTF1 complex is a novel S-phase checkpoint. Robust efforts are being made to identify more interacting partners of BMS1 and RCL1, which will contribute to revealing their precise roles in cell cycle regulation, in both ribosome biogenesis-dependent and independent manners.

Materials and methods

Zebrafish lines and maintenance

In this study, zebrafish AB line was used as WT. The mutant of *bms1^{sq163}* was obtained by ENU screening for small liver phenotype (Wang et al., 2012). The mutants of *bms1^{zju1}* and *rcl1^{zju1}* were generated using CRISPR–Cas9 technology (Zhu et al., 2021a, b). The transgenic lines Tg(*fabp10a:bms1-HA*) and Tg(*fabp10a:rcl1-myc*) were generated using Tol II transposon system via co-injecting 50 pg *Tol II* mRNA and

40 pg plasmid into 1-cell-stage WT embryos. Fish were raised and maintained according to standard procedures (Lo et al., 2003). All experiments were operated with the consent of the Animal Ethics Committee of Zhejiang University.

Cell lines and cell transfection

Human 293T, HUH7, HepG2, and Hela cells were maintained in Dulbecco's modified Eagle's medium (Meilunbio, MA0564), supplemented with 10% fetal bovine serum (FBS; ExCell Bio). Hep3B cells were maintained in minimum essential medium (Meilunbio, MA0217), supplemented with 10% FBS. All the cells were cultured with 37°C and 5% CO₂.

For transient transfection, plasmids were transfected into 293T cells using PolyJet transfection reagent (SignaGen, 71036) according to manufacturer's recommendations. After 48 h, the cells were harvested for protein extraction.

To knock down *BMS1* or *RCL1* in HUH7 and Hep3B cells, the lentiviruses of BMS1-sh08, BMS1-sh07, RCL1-sh01, RCL1-sh02, and control shRNA (shNC) were purchased from GeneChem Company for cell infection. After 24 h, the infected cells were screened by puromycin at the recommended concentration to generate stable transfected cells.

To conditionally knock down *BMS1* in Hela and HepG2 cells, shBMS1-1, shBMS1-3, and shNC were cloned into the CS-RfA-ETBsd vector (Isaji et al., 2014) and transfected into 293T cells with helper plasmids pMD2.G and psPAX2. After 48 h, lentiviruses were collected to infect Hela and HepG2 cells for 24 h, followed by a screening with Blasticidin S HCl (Beyotime, ST018) at 10 µg/ml to generate stable transfected cells. To induce the expression of shRNA, doxycycline was added to culture medium at a final concentration of 2 µg/ml and incubated for 72 h before cell harvest. All shRNA sequences are listed in [Supplementary Table S1](#).

Generation and screening of monoclonal Hela cell lines stably expressing BMS1-SFB

BMS1-SFB expression vector was generated using Gateway cloning technology through LR recombination reaction of pDonor-BMS1-attL and pLenti-CT-SFB-attR. The BMS1-SFB plasmid was transfected into 293T cells with helper plasmids psPAX2 and pMD2.G at a ratio of 1:1:1. After 48 h, the lentivirus was collected to infect Hela cells for 24 h, followed by a screening with G418 at 400 µg/ml to generate stable transfected cells. Then, single Hela cell was sorted by flow cytometry and cultured to generate monoclonal cell line. The cell lines that could stably express BMS1-SFB were selected by western blot analysis.

Plasmid construction

In our previous study, full-length cDNA sequences of zebrafish *bms1l/rcl1* and human *BMS1/RCL1* were cloned into pCS2+ expression vector (Wang et al., 2016). In this study, ZB1–ZB9 were constructed from zebrafish pCS2+–*bms1l* and cloned into pCS2+–HA expression vector, while HB1–HB4 were constructed from human pCS2+–*BMS1* and cloned into pCS2+–Flag expression vector, respectively.

Zebrafish pCS2+–Myc-Rcl1, pCS2+–Flag-Rcl1, and human pCS2+–MYC-RCL1, pCS2+–FLAG-RCL1 were constructed similarly. The pCS2+–Flag, pCS2+–HA, and pCS2+–Myc constructs were obtained from Qiang Wang (Institute of Zoology, Chinese Academy of Sciences). The pCS2+–HA-ubiquitin construct was obtained from Hui Shi (College of Animal Science, Zhejiang University). To generate transgenic fish lines with liver-specific *Bms1l* or *Rcl1* overexpression, C-terminal HA-tagged *bms1l* or myc-tagged *rcl1* and the *fabp10a* promoter were cloned into pGEMT-tol-sv40 plasmid. Lysine to arginine point mutations of zebrafish and human Rcl1 were designed in the amplifying primers, with WT pCS2+–Flag-Rcl1 used as a template. All primers used for plasmid construction are listed in [Supplementary Table S2](#).

Inhibitor treatment

The shNC or sh08 stable transfected HUH7 cells were cultured in 12-well plates for 24 h. Then, inhibitors were added to the culture medium and incubated for another 24 h before cell harvest. The inhibitors and their final concentrations were as follows: leupeptin (MCE, HY-18234A) at 30 µM, aprotinin (MCE, HY-P0017) at 6 µM, MG132 (MCE, HY-13259) at 14 µM, pepstatin A (MCE, HY-P0018B) at 2 µM, bortezomib (MCE, HY-10227) at 60 nM, tripterin (MCE, HY-13067) at 2.5 µM, and 3-MA (MCE, HY-19312) at 5 mM.

The *bms1l*^{sq163/sq163} mutant and siblings were treated with MG132 at 10 µM, bortezomib at 200 nM, pepstatin A at 2.5 µM, or leupeptin at 10 µM from 2 dpf to 5 dpf.

Cell growth curve

Cell growth was determined by Cell Counting Kit-8 (Share-Bio, SB-CCK8S) according to manufacturer's recommendations. For each time point, five repeats of each sample were set.

Northern blot analysis, 18S/28S ratio quantification, and real-time qPCR

Total RNA of human cells or zebrafish liver was extracted using Trizol Reagent (Invitrogen, 15596-026). The sequences of biotin-labeled probes P1, P2, P3, and P4 are listed in [Supplementary Table S3](#). RNA gel blot hybridization was performed as described previously (Chen et al., 2005). For 18S/28S ratio analysis, total RNA was analyzed by Agilent Bioanalysis 2100 according to manufacturer's instructions. qPCR was performed as described previously (Tao et al., 2013). The qPCR values were normalized against *elf2a* or *GAPDH* and expressed as fold change of expression. The values plotted represent mean ± SEM. All primers used for qPCR are listed in [Supplementary Table S4](#).

WISH

WISH was performed as described previously. The digoxigenin (DIG)-labeled (Roche DIG RNA Labeling Mix, 11277073901) *fabp10a* and *trypsin* probes were generated via *in vitro* transcription (Gao et al., 2019; Zhu et al., 2021b).

Protein analysis, co-IP, and antibodies

Protein extraction from zebrafish embryos or human cells, followed by western blot analysis or co-IP, was performed as described previously (Zhu et al., 2021b). Primary antibodies against Myc (ABclonal, AE070), HA (Sigma, H6908), Flag (Sigma, F1804), BMS1 (ABclonal, A15367), RCL1 (Proteintech, 15330-1-AP), fibrillarlin (Abcam, ab4566), ubiquitin (Proteintech, 10201-2-AP), PH3 (Santa Cruz, sc-8656-R), and Tubulin (Beyotime, AT819) were used in this study. Rabbit polyclonal antibodies against zebrafish Rcl1 and Bms1l and mouse monoclonal antibody betaine-homocysteine methyltransferase (Bhmt) were generated by Hangzhou HuaAn Biotechnology Company.

Cryosectioning and immunofluorescence staining

Embryos cryosectioning and immunofluorescence staining were performed as described previously (Zhu et al., 2021b). For cell immunofluorescence staining, cells cultured on coverslips were fixed with 4% paraformaldehyde (PFA) for 10 min at room temperature, followed by incubation with 0.5% Triton X-100 in phosphate-buffered saline (PBS) for 5 min at room temperature. After washing with PBS, the cells were incubated with primary antibodies for 2 h at room temperature. After washing three times with PBS, the cells were incubated with secondary antibodies and 4',6-diamidino-2-phenylindole (DAPI) for 1 h at room temperature. Images were taken under an Olympus BX61WI confocal microscope.

EdU incorporation assay

EdU (1 nM, 50 mM) was injected into the heart of 4 dpf embryos. The injected embryos were incubated at 28.5°C for 4 h, followed by fixation in 4% PFA overnight. Incorporated EdU was detected by Alexa Fluor 488 Azide (Life Technologies, A10266).

Mass spectrometry

pCS2+Flag-Rcl1 was transiently transfected into 293T cells and MG132 was added to the culture medium 24 h before harvest. Protein was extracted and incubated with Flag beads overnight at 4°C. After washing, the bound Rcl1 protein was eluted from the beads and subjected to mass spectrometry for ubiquitination sites. The detailed list of candidates can be found in [Supplementary material](#).

Statistical analysis

For statistical analysis, comparisons were made using Student's *t*-test assuming a two-tailed distribution, with significance being defined as **P* < 0.05, ***P* < 0.01, and ****P* < 0.001.

Supplementary material

[Supplementary material](#) is available at *Journal of Molecular Cell Biology* online.

Acknowledgements

We thank Dr Zeyu Sun (The First Affiliated Hospital of Zhejiang University) for technical support of mass spectrometry. We thank our colleagues Mrs Xiangfeng Shen for her expertise in zebrafish husbandry and Mrs Jingwei Lu for laboratory management.

Funding

This work was supported by grants from the National Natural Science Foundation of China (31771596 and 32000565).

Conflict of interest: none declared.

References

- Ben-Shem, A., Garreau, D.L.N., Melnikov, S., et al. (2011). The structure of the eukaryotic ribosome at 3.0 Å resolution. *Science* 334, 1524–1529.
- Billy, E., Hess, D., Hofsteenge, J., et al. (1999). Characterization of the adenylation site in the RNA 3'-terminal phosphate cyclase from *Escherichia coli*. *J. Biol. Chem.* 274, 34955–34960.
- Billy, E., Wegierski, T., Nasr, F., et al. (2000). Rcl1p, the yeast protein similar to the RNA 3'-phosphate cyclase, associates with U3 snoRNP and is required for 18S rRNA biogenesis. *EMBO J.* 19, 2115–2126.
- Bohnsack, K.E., and Bohnsack, M.T. (2019). Uncovering the assembly pathway of human ribosomes and its emerging links to disease. *EMBO J.* 38, e100278.
- Boisvert, F.M., van Koningsbruggen, S., Navascues, J., et al. (2007). The multifunctional nucleolus. *Nat. Rev. Mol. Cell Biol.* 8, 574–585.
- Chaker-Margot, M., Barandun, J., Hunziker, M., et al. (2017). Architecture of the yeast small subunit processome. *Science* 355, eaal1880.
- Charette, J.M., and Baserga, S.J. (2010). The DEAD-box RNA helicase-like Utp25 is an SSU processome component. *RNA* 16, 2156–2169.
- Chen, J., Ruan, H., Ng, S.M., et al. (2005). Loss of function of *def* selectively up-regulates $\Delta 113p53$ expression to arrest expansion growth of digestive organs in zebrafish. *Genes Dev.* 19, 2900–2911.
- Cheng, J., Kellner, N., Berninghausen, O., et al. (2017). 3.2-Å-resolution structure of the 90S preribosome before A1 pre-rRNA cleavage. *Nat. Struct. Mol. Biol.* 24, 954–964.
- Delprato, A., Al, K.Y., Perebaskine, N., et al. (2014). Crucial role of the Rcl1p–Bms1p interaction for yeast pre-ribosomal RNA processing. *Nucleic Acids Res.* 42, 10161–10172.
- Elia, A.E., Boardman, A.P., Wang, D.C., et al. (2015). Quantitative proteomic atlas of ubiquitination and acetylation in the DNA damage response. *Mol. Cell* 59, 867–881.
- Fan, W.H., Hou, Y., Meng, F.K., et al. (2011). Proteasome inhibitor MG-132 induces C6 glioma cell apoptosis via oxidative stress. *Acta Pharmacol. Sin.* 32, 619–625.
- Gao, C., Huang, W., Gao, Y., et al. (2019). Zebrafish *hhex*-null mutant develops an intrahepatic intestinal tube due to de-repression of *cdx1b* and *pdx1*. *J. Mol. Cell Biol.* 11, 448–462.
- Henras, A.K., Plisson-Chastang, C., O'Donohue, M.F., et al. (2015). An overview of pre-ribosomal RNA processing in eukaryotes. *Wiley Interdiscip. Rev. RNA* 6, 225–242.
- Horn, D.M., Mason, S.L., and Karbstein, K. (2011). Rcl1 protein, a novel nuclease for 18S ribosomal RNA production. *J. Biol. Chem.* 286, 34082–34087.
- Isaji, T., Im, S., Gu, W., et al. (2014). An oncogenic protein golgi phosphoprotein 3 up-regulates cell migration via sialylation. *J. Biol. Chem.* 289, 20694–20705.
- Jiaze, Y., Sinan, H., Minjie, Y., et al. (2022). Rcl1 suppresses tumor progression of hepatocellular carcinoma: a comprehensive analysis of bioinformatics and in vitro experiments. *Cancer Cell Int.* 22, 114.

- Karbstein, K., Jonas, S., and Doudna, J.A. (2005). An essential GTPase promotes assembly of preribosomal RNA processing complexes. *Mol. Cell* 20, 633–643.
- Khatter, H., Myasnikov, A.G., Natchiar, S.K., et al. (2015). Structure of the human 80S ribosome. *Nature* 520, 640–645.
- Kornprobst, M., Turk, M., Kellner, N., et al. (2016). Architecture of the 90S pre-ribosome: a structural view on the birth of the eukaryotic ribosome. *Cell* 166, 380–393.
- Lo, J., Lee, S., Xu, M., et al. (2003). 15000 unique zebrafish EST clusters and their future use in microarray for profiling gene expression patterns during embryogenesis. *Genome Res.* 13, 455–466.
- Maclaren, A.P., Chapman, R.S., Wyllie, A.H., et al. (2001). p53-dependent apoptosis induced by proteasome inhibition in mammary epithelial cells. *Cell Death Differ.* 8, 210–218.
- Shahshahan, M.A., Beckley, M.N., and Jazirehi, A.R. (2011). Potential usage of proteasome inhibitor bortezomib (Velcade, PS-341) in the treatment of metastatic melanoma: basic and clinical aspects. *Am. J. Cancer Res.* 1, 913–924.
- Singh, S., Vanden, B.A., Miller, L., et al. (2021). Nucleolar maturation of the human small subunit processome. *Science* 373, j5338.
- Sloan, K.E., Mattijssen, S., Lebaron, S., et al. (2013). Both endonucleolytic and exonucleolytic cleavage mediate ITS1 removal during human ribosomal RNA processing. *J. Cell Biol.* 200, 577–588.
- Tanaka, N., Smith, P., and Shuman, S. (2011). Crystal structure of Rcl1, an essential component of the eukaryal pre-rRNA processosome implicated in 18S rRNA biogenesis. *RNA* 17, 595–602.
- Tao, B., Lo, L.J., Peng, J., et al. (2020). rDNA subtypes and their transcriptional expression in zebrafish at different developmental stages. *Biochem. Biophys. Res. Commun.* 529, 819–825.
- Tao, T., Shi, H., Huang, D., et al. (2013). Def functions as a cell autonomous factor in organogenesis of digestive organs in zebrafish. *PLoS One* 8, e58858.
- Tsubuki, S., Saito, Y., Tomioka, M., et al. (1996). Differential inhibition of calpain and proteasome activities by peptidyl aldehydes of di-leucine and tri-leucine. *J. Biochem.* 119, 572–576.
- Wang, M., Anikin, L., and Pestov, D.G. (2014). Two orthogonal cleavages separate subunit RNAs in mouse ribosome biogenesis. *Nucleic Acids Res.* 42, 11180–11191.
- Wang, Y., Luo, Y., Hong, Y., et al. (2012). Ribosome biogenesis factor Bms1-like is essential for liver development in zebrafish. *J. Genet. Genomics* 39, 451–462.
- Wang, Y., Zhu, Q., Huang, L., et al. (2016). Interaction between Bms1 and Rcl1, two ribosome biogenesis factors, is evolutionally conserved in zebrafish and human. *J. Genet. Genomics* 43, 467–469.
- Wegierski, T., Billy, E., Nasr, F., et al. (2001). Bms1p, a G-domain-containing protein, associates with Rcl1p and is required for 18S rRNA biogenesis in yeast. *RNA* 7, 1254–1267.
- Wells, G.R., Weichmann, F., Colvin, D., et al. (2016). The PIN domain endonuclease Utp24 cleaves pre-ribosomal RNA at two coupled sites in yeast and humans. *Nucleic Acids Res.* 44, 5399–5409.
- Woolford, J.J., and Baserga, S.J. (2013). Ribosome biogenesis in the yeast *Saccharomyces cerevisiae*. *Genetics* 195, 643–681.
- Yerlikaya, A., Okur, E., Eker, S., et al. (2010). Combined effects of the proteasome inhibitor bortezomib and Hsp70 inhibitors on the B16F10 melanoma cell line. *Mol. Med. Rep.* 3, 333–339.
- Zhao, S., Huang, D., and Peng, J. (2021). Nucleolus-localized Def-CAPN3 protein degradation pathway and its role in cell cycle control and ribosome biogenesis. *J. Genet. Genomics* 48, 955–960.
- Zhu, Q., Tao, B., Chen, H., et al. (2021a). Rcl1 depletion impairs 18S pre-rRNA processing at the A1-site and up-regulates a cohort of ribosome biogenesis genes in zebrafish. *Nucleic Acids Res.* 49, 5743–5759.
- Zhu, Y., Wang, Y., Tao, B., et al. (2021b). Nucleolar GTPase Bms1 displaces Ttf1 from RFB-sites to balance progression of rDNA transcription and replication. *J. Mol. Cell Biol.* 13, 902–917.

Received February 25, 2023. Revised July 3, 2023. Accepted July 13, 2023.

© The Author(s) (2023). Published by Oxford University Press on behalf of *Journal of Molecular Cell Biology*, CEMCS, CAS.

This is an Open Access article distributed under the terms of the Creative Commons Attribution-NonCommercial License (<https://creativecommons.org/licenses/by-nc/4.0/>), which permits non-commercial re-use, distribution, and reproduction in any medium, provided the original work is properly cited. For commercial re-use, please contact journals.permissions@oup.com